

Mitigation of Global Navigation Satellite System Cycle Slips Due to Scintillation Using Radio Backpropagation

Brian Breitsch* | Jade Morton

Smead Aerospace Engineering Sciences,
University of Colorado, Boulder,
Colorado, United States

Correspondence

Brian Breitsch
CCAR
University of Colorado, Boulder
3775 Discovery Drive, 429 UCB
Boulder, CO 80303
Email: brianbreitsch@gmail.com

Abstract

Measurements of signals from satellites from global navigation satellite systems are an important tool not only for precision navigation and timing applications, but also for various scientific and remote-sensing applications such as ionosphere monitoring and atmosphere probing using radio occultation. When traveling through turbulent patches of the Earth's ionosphere, these signals can experience scintillation, which is characterized by rapid fluctuations in the amplitude and phase of the received signal. In addition to these fluctuations, the signal can undergo phase transitions that induce cycle slips in the resulting phase measurement. When left uncorrected, cycle slips can lead to large errors in positioning and remote-sensing applications. In this work, we determine how backpropagation based on a single-phase screen model of the ionosphere can help to limit the occurrence of these cycle slips. This approach is applicable for batch post-processing of measurements. Furthermore, our results when applying the method to both simulations and real-life data suggest that backpropagation can correct many of the cycle slips that are generated during severe scintillation.

Keywords

backpropagation, cycle slips, global navigation satellite system, scintillation

Cycle slips in signals from global navigation satellite systems (GNSSs) are rapid and discrete changes in the measured phase that can be the result of noise, receiver processing, and propagation. When left uncorrected, cycle slips can lead to errors in precision navigation and remote sensing applications. Banville et al. (2010) identified cycle slips occurring during ionosphere plasma bubble events as particularly challenging. In these scenarios, the received signal displays fluctuations due to interference from scattered signal components and can contain noise and phase transitions that may result in many cycle slips in the unwrapped phase measurements (Breitsch et al., 2020). At the same time, large variations in the refractive ionosphere phase component can obscure these events, making their detection a difficult task.

While there has been extensive characterization of scintillation-induced carrier-phase errors through their standard deviation, or σ_ϕ index, such

characterizations do not fully capture the magnitude of errors that caused by diffraction by the introduction of cycle slips. Simulation results published by Breitsch et al. (2020) revealed that for strong scintillation ($S_4 \approx 0.8$), cumulative phase errors due to cycle slips follow a Skellam distribution with a 95% confidence interval lying between ± 11 cycles over five minutes. When undetected, these errors can be detrimental to pseudorange smoothing algorithms (Myer & Morton, 2018). They can also lead to false confidence with algorithms such as (Vadakke Veetil et al., 2020) that base measurement integrity on receiver tracking indicators. Various techniques have been pioneered for cycle slip mitigation under harsh signal conditions, including detection in detrended phase (Rovira-Garcia et al., 2020), adaptive filtering of phase measurements (Wang et al., 2020), and batch estimation using Gaussian processes (Breitsch, 2021). While these methods can be effective in certain situations, they all rely on statistical detection of slips as outliers and are ultimately susceptible to the severity of signal phase fluctuations.

In this work, we demonstrate a cycle slip mitigation approach that shows some promise under severe scintillation conditions. In this approach, radio backpropagation of the received complex signal is performed assuming a phase screen model for ionosphere propagation. Reductions in cycle slips and diffraction errors were based on the premise that the propagation channel was well-approximated by a single-phase-screen model, because in this case the signal contains no diffractive effects when evaluated at the phase screen. This also suggests the backpropagation operation, which maps a complex signal back to some point before diffraction effects can develop, can be a useful tool in “undoing” some of the effects of scintillation. Radio backpropagation has been used previously to locate irregularities in the ionosphere using radio occultation receivers (Sokolovskiy et al., 2002; Carrano et al. 2011). The phase screen propagation model has been used extensively to characterize the impact of scintillation on GNSS measurements (Ghafoori & Skone, 2015). Breitsch et al. (2020) used the phase screen model specifically to assess the impact of scintillation-induced cycle slips. While the theory behind phase screen models predicts that backpropagation might be used to mitigate the effects of scintillation, its use may be limited by the single-phase-screen assumption and practical issues concerning noise and phase variations associated with non-ionospheric sources. Our intent in this paper is to determine how effectively scintillation-induced cycle slips could be mitigated despite these limitations. We also note that, while the approach we present in this paper does not work in real-time, it does permit post-processing algorithms to process carrier measurements that are less noisy and with fewer cycle slips. Furthermore, this approach also lays the groundwork for potential near-real-time implementations of a back-propagation filter.

In Section 1, we begin by introducing the phase screen principle for modeling radio propagation through the ionosphere. We then discuss the necessary model parameters, how backpropagation may be applied to filter GNSS carrier phase measurements, and how one might simulate this process. In Section 2, we first apply this method to simulated measurements to evaluate the impact of different noise levels and non-ionospheric phase variations on the algorithm performance. Then, in Section 3, we evaluate real measurements on the GPS L1, L2, and L5 frequencies from diffractive ionosphere scintillation detected at a receiver near Hong Kong, which lies at around 22.4° latitude and often measures strong ionosphere scintillation. We show how the backpropagation algorithm can eliminate most of the slip events that occur due to scintillation.

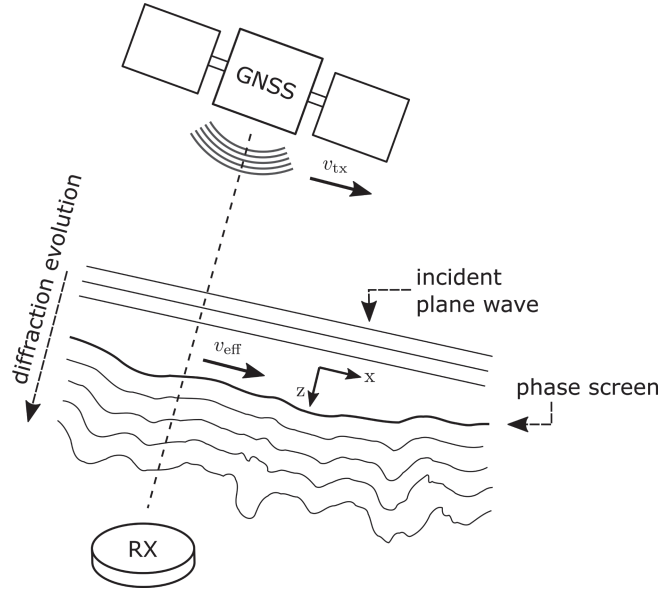


FIGURE 1 Illustration of the geometry of the phase screen model

1 | BACKGROUND

1.1 | Phase Screen Theory

Phase screen models have become useful tools for simulating diffraction of a signal as it propagates through irregular ionosphere structures. Following the development described by Carrano et al. (2011), we consider a case in which the waveform can be adequately modeled as a plane wave propagating through multiple phase screens. As shown in Figure 1, we consider a coordinate frame centered at the receiving antenna with the z -axis oriented along the direction from the GNSS satellite toward a ground receiver, with the phase screen specified as a function along the x -axis. In this geometry, v_{eff} is the *effective scan velocity* of the GNSS ray through the ionosphere structure, which takes into account the satellite/receiver motion and irregularity drift. In the spatial domain, the propagating GNSS wave at one of these screens is described by its complex amplitude $u(x, z)$, and the incident wave at the phase screen is assumed to be a plane wave (i.e. $|u(x, z)| = 1$). After this plane wave passes through the phase screen, which imparts its phase structure onto the propagating wave, diffractive fluctuations in the signal evolve as it propagates away from the screen as shown in Figure 1.

Rino (2011) described a two-step procedure for implementing the forward phase-screen model. In the first step, the complex wave amplitude before the phase screen $u(x, z_n^-)$ is modified by a phase perturbation $\Delta\phi$, which is due to the medium structure in the volume pertaining to the phase screen. This can be expressed as indicated in Equation (1):

$$u(x, z_n^+) = u(x, z_n^-) \exp(i\Delta\phi(x, z_n)) \quad (1)$$

where Equation (2):

$$\Delta\phi(x, z_n) = \int_{z_n}^{z_{n+1}} \lambda r_e N_e(x, \xi) d\xi \quad (2)$$

is the phase imparted to the signal, $r_e = 2.8179403 \times 10^{-15}$ is the classical electron radius, and N_e denotes the ionosphere plasma density. The second step is to propagate the modified wave $u(x, z_n^+)$ to the next phase screen. This is done by first applying the Fourier transform in the dimension that is transverse to the propagating field and then applying the forward propagation operator from the current to the next phase screen. Finally, the inverse Fourier transform is applied to recover the field complex amplitude at the next phase screen. These steps are outlined as follows in Equations (3), (4), and (5):

$$U(k_x, z_n^+) = \int_{-\infty}^{\infty} u(x, z_n^+) \exp(-ik_x x) dx \quad (3)$$

$$U(k_x, z_{n+1}^-) = U(k_x, z_n^+) \exp\left(i(k^2 - k_x^2)^{\frac{1}{2}} \Delta z\right) \quad (4)$$

$$u(x, z_{n+1}^-) = \frac{1}{2\pi} \int_{-\infty}^{\infty} U(k_x, z_{n+1}^-) \exp(ik_x x) dk_x \quad (5)$$

where k is the spatial wavenumber and k_x is the spatial wavenumber in the x -direction.

While the physical phase screen theory described above was developed in the spatial domain, our actual GNSS receiver measurements are in the form of time series. Conversion of the spatial signal to a time series of a received signal can be done by assuming an effective scan velocity v_{eff} of the received signal ray path through the ionosphere structure (Rino et al., 2018) as shown in Equation (6):

$$x = v_{\text{eff}} \cdot t \quad (6)$$

A convenient simplification of this formula is discussed in Rino et al. (2018). By taking $\mu = k_x \rho_f$, where ρ_f is the Fresnel scale, we can rescale the phase screen so that it is in normalized units. To distinguish this new scaling, we refer to the wave complex amplitude as $\psi(t, z)$. In these scaled units, Equations (3), (4), and (5) become Equations (7), (8), and (9):

$$\Psi(\mu, z_n^+) = \int_{-\infty}^{\infty} \psi(t, z_n^+) \exp(-i\omega t) dt \quad (7)$$

$$\Psi(\omega, z_{n+1}^-) = \Psi(\omega, z_n^+) \exp\left(-i \frac{(\omega \cdot \rho / v_{\text{eff}})^2}{2}\right) \quad (8)$$

$$\psi(t, z_{n+1}^-) = \frac{1}{2\pi} \int_{-\infty}^{\infty} \Psi(\omega, z_{n+1}^-) \exp(i\omega t) d\omega \quad (9)$$

Finally, given a received complex field, the backpropagation operation is simply an undoing of the process described by Equations (7) and (8):

$$\Psi(\omega, z_{n+1}^+) = \int_{-\infty}^{\infty} \psi(t, z_{n+1}^-) \exp(-i\omega t) dt \quad (10)$$

$$\Psi(\omega, z_{n+1}^-) = \Psi(\omega, z_{n+1}^+) \exp\left(i \frac{(\omega \cdot \rho / v_{\text{eff}})^2}{2}\right) \quad (11)$$

$$\psi(t, z_n^-) = \frac{1}{2\pi} \int_{-\infty}^{\infty} \Psi(\omega, z_{n+1}^-) \exp(i\omega t) d\omega \quad (12)$$

where $\psi(t, z_{n+1}^+)$ is the received complex signal and $\psi(t, z_n^-)$ is the backpropagated signal. Note that, in this process, ρ / v_{eff} is the only parameter that remains undetermined.

1.2 | Phase Screen Parameters

In this subsection, we briefly discuss the simulation of the phase screen structure. Models such as those described by Carrano et al. (2011) and Rino (2011) specify the power spectral density of the stochastic process from which the phase screen structure is assumed to be drawn. In this work, we will consider the two-component power law spectrum for modeling strong equatorial ionosphere scintillation. The power spectrum specifying the phase screens requires four parameters: U , μ_0 , p_1 , and p_2 as indicated in Equation (13):

$$P_{\Delta\phi}(\mu) = C_{pp} \begin{cases} \mu^{-p_1} & \mu \geq 1 \\ \mu_0^{p_2-p_1} \mu^{-p_2} & \mu < 1 \end{cases} \quad (13)$$

where, as in Equation (14):

$$C_{pp} = \begin{cases} U & \mu_0 \geq 1 \\ U / \mu_0^{p_2-p_1} & \mu_0 < 1 \end{cases} \quad (14)$$

The universal strength parameter U determines the magnitude of plasma irregularities relative to the background density and generally describes the strength of amplitude and phase fluctuations in the resulting scintillation. The remaining parameters μ_0 , p_1 , and p_2 , respectively, define the break scale and slopes of a two-component inverse power law spectrum derived from the statistical structure of the ionosphere irregularities. For an in-depth discussion readers are referred to Rino et al. (2018).

The parameter ρ / v_{eff} is the ratio of the first Fresnel radius ρ to the effective scan velocity v_{eff} ; its value is associated with the time scale of diffractive fluctuations. This set of parameters is defined for a given signal frequency and then mapped to physically consistent values for other frequencies. In other words, if ρ_i is the Fresnel scale corresponding to carrier frequency f_i then $\rho_1 / v_{\text{eff}} = \rho_2 / v_{\text{eff}} \cdot \sqrt{f_1 / f_2}$. Note that, for the simulations presented in Section 2, the stochastic phase screen structure is initialized using the same random seed so that signal fluctuations across different frequencies are consistent with propagation through the same random structure.

Xu (2019) suggested mapping these model parameters to two more intuitive parameters, i.e., the scintillation index S_4 and the decorrelation time τ , which are commonly used in characterizing equatorial scintillation (c.f. Humphreys et al., 2010; de Oliveira Moraes et al. 2012). In this study, we used S_4 and τ to characterize the different scintillation scenarios under consideration, where S_4 is defined as per usual as the normalized deviation of signal intensity and the decorrelation time is defined as the point at which the intensity of the autocorrelation drops to $1/e$ of its peak value. Xu et al. (2020) found that for ground stations at low latitudes, μ_0 , p_1 , and p_2 remain close to their nominal values of 0.8, 2.7, and 3.6, respectively.

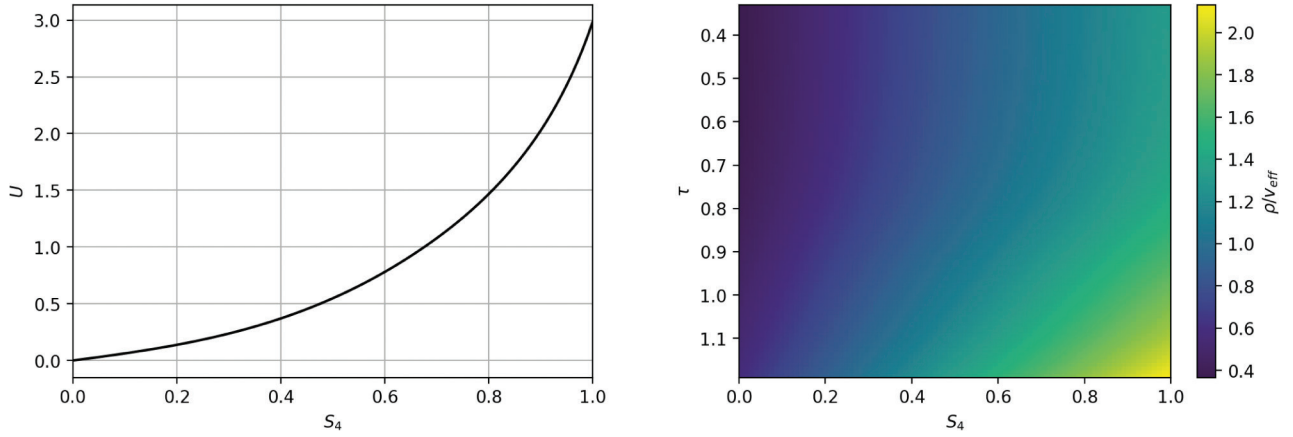


FIGURE 2 Illustration of the correspondence between S_4 and U (left panel) and the bi-linear relationship between ρ/v_{eff} , S_4 , and τ (right panel)

TABLE 1

Scintillation Phase Screen Parameters (for L1 Signal)

These parameters are used for the simulations shown in Section 2.

| S_4 | τ | U | ρ/v_{eff} |
|-------|--------|------|-----------------------|
| 0.5 | 0.8 | 0.55 | 1.21 |
| 0.65 | 0.8 | 0.92 | 1.33 |
| 0.80 | 0.8 | 1.47 | 1.49 |

Meanwhile, the parameters U and ρ/v_{eff} can capture nearly all the observed variation in the scintillation characteristics. Mappings between the parameters were derived empirically by simulating scintillation for various values of U and ρ/v_{eff} and then computing the corresponding S_4 and τ from the resulting simulated intensity. The results of these studies revealed that the value of S_4 has a direct correspondence with U , while ρ/v_{eff} can be described as a bi-linear dependence on S_4 and τ . Figure 2 illustrates the relationships between these parameters. These relationships are used to determine the simulation parameter groups shown in Table 1 and to estimate ρ/v_{eff} from S_4 and τ in the real scintillation data set as described in Section 3.

1.3 | Backpropagation Algorithm

We can model the phase used for GNSS signal carrier phase measurements as shown in Equation (15):

$$\phi_k(t) = \phi_G(t) - \phi_{I,k}(t) + \eta_k(t) \quad (15)$$

where

- k denotes dependence on the signal carrier frequency f_k with wavelength λ_k ;
- ϕ_G includes the non-ionospheric phase components that contain the non-dispersive effects of satellite/receiver clocks and positions, propagation through the troposphere, and others;

- $\phi_{\mathcal{I}}$ is the ionosphere phase term, consisting of contributions from both ionosphere total electron content (TEC) and scintillation; and
- η is noise

We further model the ionosphere phase component as indicated in Equation (16):

$$\phi_{\mathcal{I},k}(t) = \frac{2\pi}{c} \frac{\kappa}{f_k} \text{TEC}(t) + \phi_{s,k}(t) \quad (16)$$

where

- TEC is the ionosphere total electron content along the ray path, measured in TEC units (TECu) where $1\text{TECu} = 1 \times 10^{16} \frac{\text{electrons}}{\text{m}^2}$
- $\kappa \approx 40.308 \times 10^{16} \frac{\text{s}^2}{\text{TECu}}$ is a constant

On the right-hand-side of Equation (16), the first term is the first-order ionosphere effect and the second term $\phi_{s,k}$ is the remaining effect due to scintillation.

The backpropagation algorithm can be applied to a window of sufficiently high-rate signal carrier phase and amplitude measurements. While use of the term “sufficiently high” to describe the rate depends on the propagation geometry, generally 50–100 Hz measurements are enough for a standard ground receiver. Applying the algorithm requires that we have isolated most of the signal variations due to the ionosphere. For real measurements, isolating this scintillation carrier phase (denoted $\tilde{\phi}$) involves approximate estimation and removal of non-ionospheric phase components $\phi_{\mathcal{G}}$, which can be achieved using satellite clock/orbits and a coarse receiver clock/position solution. Note that any large phase trends (but not biases) may have an impact on the performance of the backpropagated algorithm; this will be quantified later in Section 2. It may also be necessary to isolate ionosphere fluctuations in the signal amplitude (denoted \tilde{A}). This can be accomplished by dividing the measured signal amplitude by a moving average that captures the nominal amplitude trend. Note that this process is performed before measuring the amplitude scintillation index S_4 .

From the detrended amplitude \tilde{A} we can compute the values τ and S_4 . These values can then be mapped to ρ / v_{eff} . An average ρ / v_{eff} value can be used if it does not change too much over the measurement window. Then, having isolated the ionosphere signal fluctuations in \tilde{A} and $\tilde{\phi}$, we form the complex received signal $\tilde{\psi}$ and apply the backpropagation algorithm using the derived value of ρ / v_{eff} . Finally, to obtain the final filtered measurements, we can return the estimated non-ionospheric components to the overall sum. Figure 3 illustrates these steps along with their respective data inputs.

1.4 | Simulating Measurements

The process of simulating a scintillation phase amounts to simulating the second term on the right-hand-side of Equation (15). Given a set of phase screen parameters and initial signal frequencies, the scintillation model generates a consistent set of phase screens $\phi_{\text{TEC},k}$ and realizations ψ_k of the complex field at the receiving antenna. In our simulations, we consider the true (noise-free) phase and amplitude of the signal to be as indicated in Equation (17) and Equation (18):

$$\phi_k(t) = \text{unwrap}(\angle \psi_k(t)) \quad (17)$$

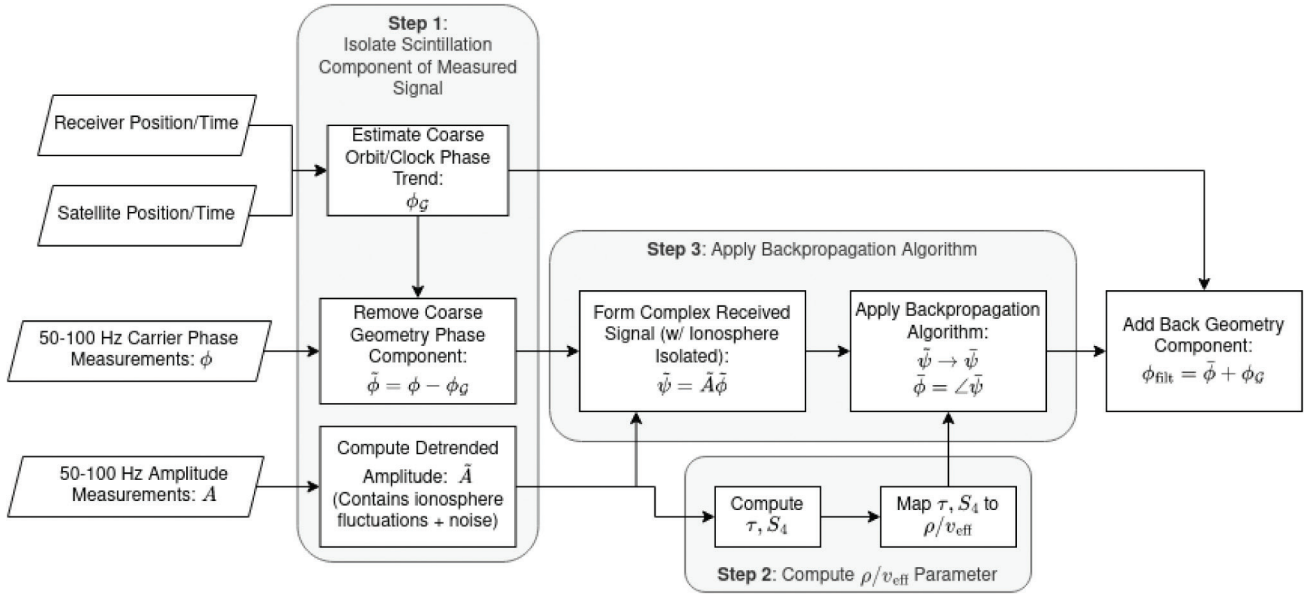


FIGURE 3 Block diagram depicting the steps involved when using the scintillation backpropagation algorithm to correct phase measurements

$$A_k(t) = |\psi_k(t)| \quad (18)$$

The time series $\phi_k(t)$ effectively simulates Equation (15), assuming that $\phi_G(t)$ is zero. We also assume that the second term (ionosphere TEC) is equal to the phase screen contribution $\phi_{\text{TEC},k}(t)$.

Figure 4 includes examples of noise-free simulated scintillation intensity and phase time series for a case exhibiting moderately strong equatorial scintillation for all three GPS signal frequencies. Note that the phase measurements were scaled to be in TEC units. The similarity between the phases seen in all three phases is consistent with the attribution of most of variation to the phase screens, which are nearly identical among the three frequencies. The persistent discrepancies between the phases are due to diffraction-induced phase transitions.

1.5 | Adding Noise

We consider a baseline carrier-to-noise density ratio $\overline{C/N_0}$ to be the relevant parameter for determining the impact of noise on cycle slip occurrence. $\overline{C/N_0}$ is defined as the carrier-to-noise density ratio that would be measured in the absence of any scintillation diffraction. In order to simulate the impact of different C/N_0 , we generate noise according to Equation (19):

$$\eta_k(t) \sim \mathcal{N}(0, \sigma^2) \quad \sigma = \frac{B}{\overline{C/N_0}} \quad (19)$$

$\eta_k(t)$ are assumed to be independent random variables drawn from the zero-mean circular complex normal distribution with variance σ^2 . We assume the noise bandwidth B is equal to $1/T$, where $T = 0.01$ seconds is the measurement integration time and sampling interval. The noisy simulations of phase and amplitude measurements are then given by Equation (20) and Equation (21):

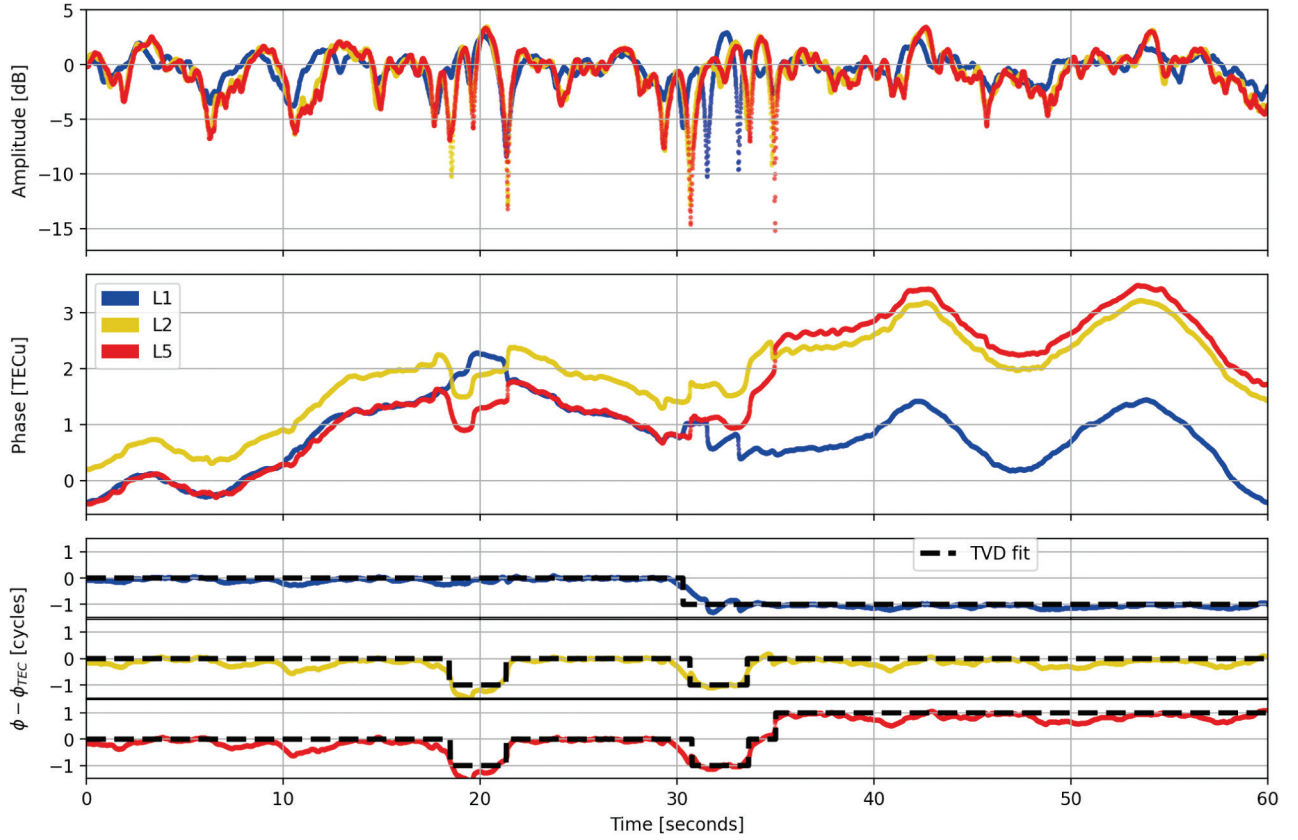


FIGURE 4 Simulated scintillation amplitude (first panel) and phase (second panel) measurements corresponding to L1, L2, and L5 frequencies for a strong scintillation. The phase in the second panel has been scaled to TECu. The third panel shows the simulated diffraction residuals obtained by subtracting the phase screen from the simulated phase measurements. The black dashed lines show the fit used to identify cycle slip occurrences.

$$\phi_k(t) = \text{unwrap}\left(\angle(\psi_k(t) + \epsilon_k(t))\right) \quad (20)$$

$$A_k(t) = |\psi_k(t) + \epsilon_k(t)| \quad (21)$$

1.6 | Identifying Cycle Slips in Simulations

It will also be necessary to identify cycle slip occurrences in the simulations. To do so, we use the total variation denoising (TVD) procedure described in Breitsch et al. (2020) in which a piece-wise constant fit is applied to the diffraction residual (defined as the measured phase minus the $\mathcal{G}(t)$ and $\text{TEC}(t)$ terms); slips are identified as sufficiently large jumps in this fit. The bottom panel of Figure 4 illustrates the diffraction residuals and corresponding piece-wise fit to the residuals. The jumps in the fit (one on L1, four on L2, and five on L5) correspond to the definition of cycle slip occurrences used in this work.

2 | SIMULATION RESULTS

In this section, we develop results on the efficacy of backpropagation under two types of scenarios: (1) when the signal has low C / N_0 or (2) when there is variation,

or Doppler, in the non-ionospheric phase components ϕ_G . To do this, we first simulate phase and amplitude measurements using the phase screen scintillation model. For the $\phi_G(t)$ term, we add a linear phase trend corresponding to a value of Doppler in m/s, which we denote $\Delta\mathcal{G}$. For each scenario (i.e., a particular S_4 , C/N_0 , or $\Delta\mathcal{G}$ value), we ran 100 simulations of 10 minutes each, which provided statistically significant results to as low as at least 0.1 slips per minute given that slip occurrence is assumed to follow a Poisson process. We then applied backpropagation using the simulated phase and amplitude measurements. We identified and counted the slip occurrences both before and after applying backpropagation.

Figure 5 shows the rates of cycle slip occurrence both before and after applying backpropagation under varying C/N_0 levels and for different scintillation strengths. We see that at high C/N_0 there are essentially zero slips in the phase after applying backpropagation, regardless of the S_4 value. However, below

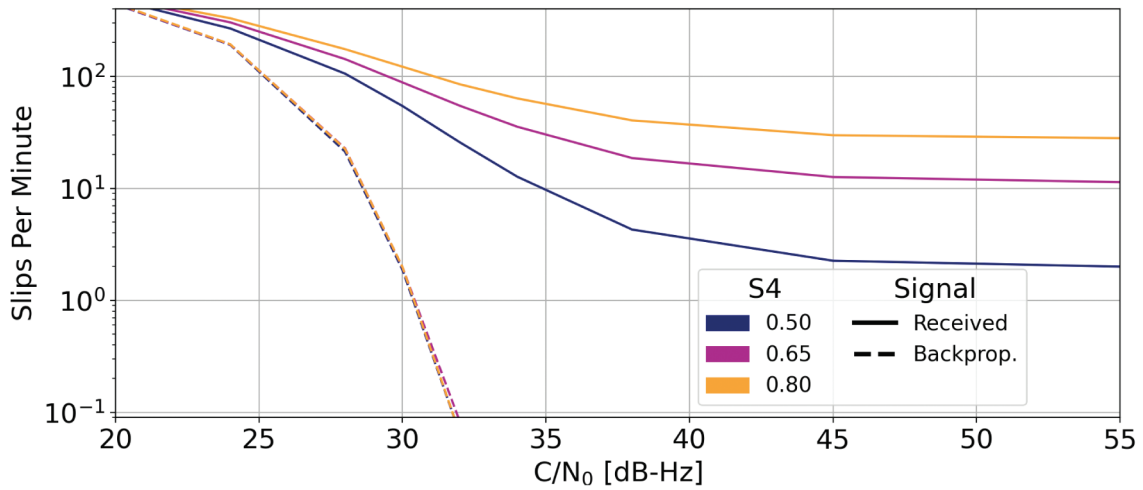


FIGURE 5 The occurrence rates of cycle slips
Shown here are findings obtained from simulated measurements before (solid lines) and after (dashed lines) applying backpropagation, as related to different signal C/N_0 values. Different colored lines are used to indicate the different scintillation strengths as defined by S_4 .

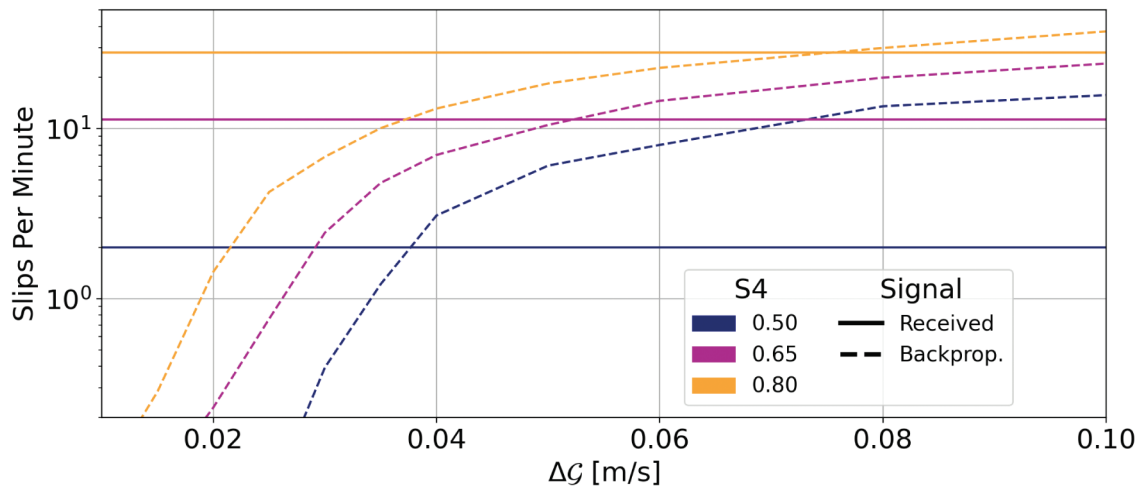


FIGURE 6 The occurrence rate of cycle slips
The findings shown here are similar to those shown in Figure 5 with simulated measurements before and after applying backpropagation under different levels of non-ionospheric Doppler.

around 30 dB-Hz, backpropagation performance begins to deteriorate equally in all scintillation scenarios. Similar to Figure 5, Figure 6 documents the slip occurrence rates before and after applying backpropagation, in this case in response to different levels of contamination of the linear Doppler trend for $\phi_g(t)$. Here, we see that as the residual trend grows larger, the backpropagation performance deteriorates, with performance growing worse more rapidly in those cases with stronger scintillation.

3 | REAL-WORLD DATA

In this section we discuss results of applying backpropagation to real-world data collected on GPS L1, L2, and L5 bands during a scintillation event for a receiver near Hong Kong. The scintillation event lasts around 40 minutes. Figure 7 shows the measured C/N_0 and detrended phase during the event, along with estimates of the ρ/v_{eff} parameter based on the observed S_4 and τ values. To estimate the non-ionospheric phase component, we used a surveyed receiver position, precise satellite orbit and clock products, and the receiver clock bias estimated using measurements from signals not experiencing scintillation. We applied backpropagation to successive 500 second windows starting at 716 minutes using $\rho/v_{\text{eff}} = 0.8$, which is approximately the average value during the scintillating part of the data set.

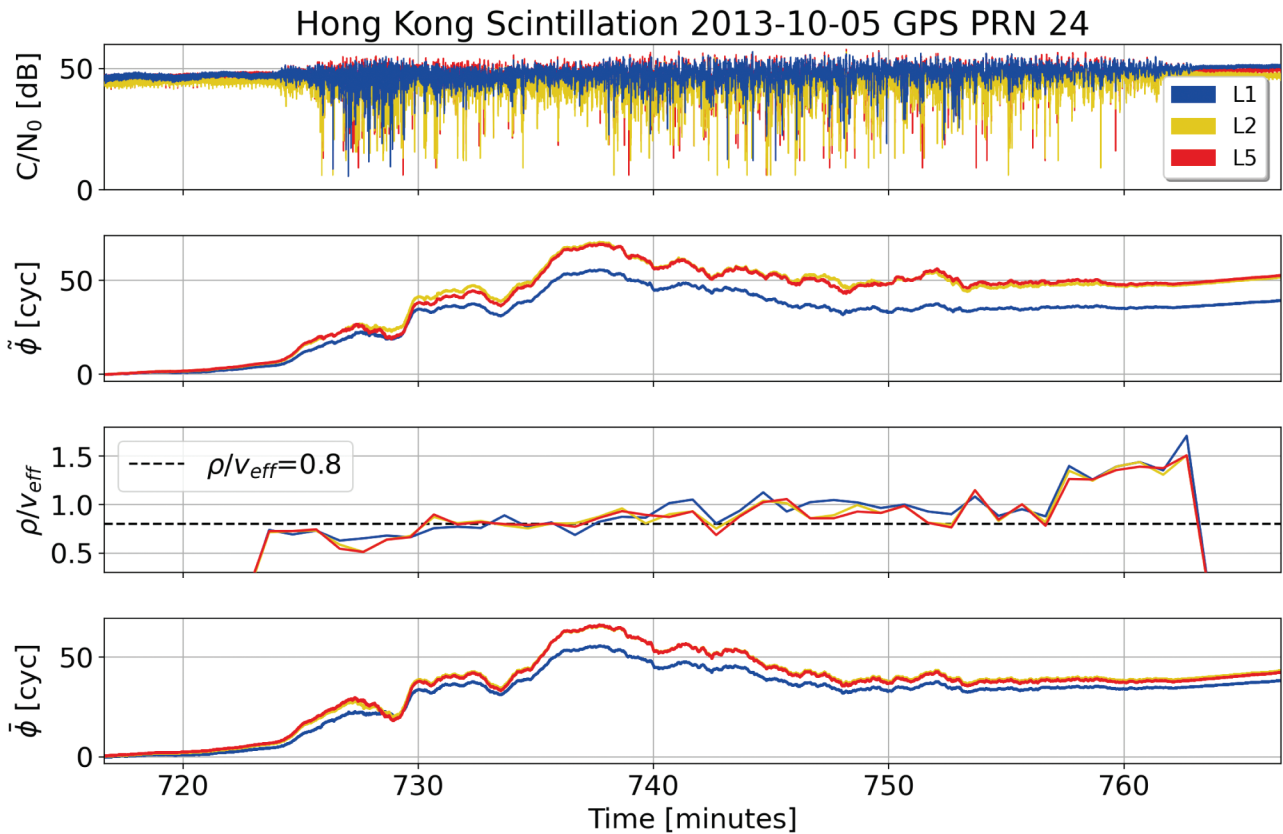


FIGURE 7 Signal C/N_0 (top panel), detrended phase (second panel), the ρ/v_{eff} parameter (third panel), and the detrended phase after applying the backpropagation procedure (fourth panel) for GPS L1, L2, and L5 measurements during a scintillation event for a receiver near Hong Kong.

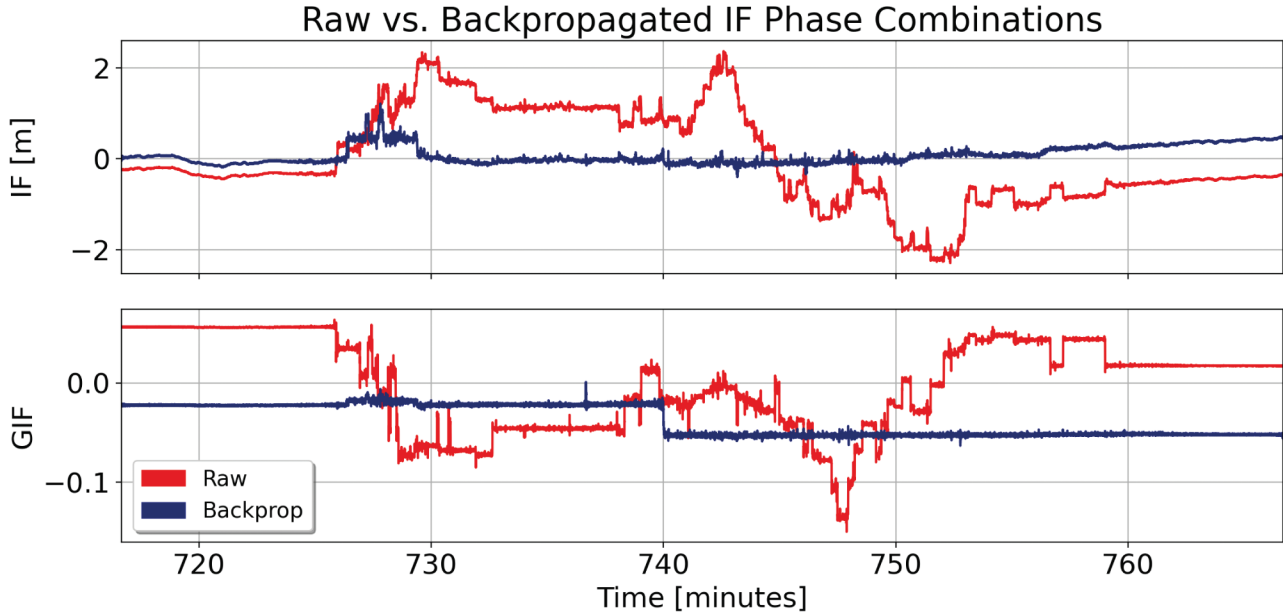


FIGURE 8 The ionosphere-free (IF) and geometry-ionosphere-free (GIF) phase combinations before (red) and after (blue) applying backpropagation

It is difficult to assess the performance of backpropagation for real-life data because we have no truth reference for the occurrence of cycle slips. A good proxy would be to consider the smoothness of phase combinations obtained using the phase both before and after applying the algorithm. Figure 8 documents ionosphere-free (IF) and geometry-ionosphere-free (GIF) phase combinations obtained before and after applying backpropagation. Given that the carrier phase is in cycles, the coefficients to construct these combinations are (12.228, -1.473 , -3.796) for IF and (0.125, -0.528 , 0.412) for GIF. Note that the non-ionospheric phase component has not been added back to the filtered phase measurements, so the IF combination should also be nearly flat.

We observe a significant reduction in the number of jumps in both combinations after performing backpropagation. This suggests that, at least for most of the event, backpropagation is an effective way to eliminate the impact of cycle slips due to scintillation. However, there are still some slip occurrences in the data, which can be seen by the subtle jumps in the IF combinations, notably around 730 minutes. We note that the baseline C/N_0 is around 45 dB-Hz for these data, so the impact of noise is not a likely factor contributing to these slip occurrences. Also, based on small overall variations in the IF combination, the geometric range has been accurately detrended overall, but it is possible that some other unknown factors, like multipath, contaminated the detrended phase at that time. Interestingly, this period corresponds to a slight dip in the computed ρ/v_{eff} and to a period of particularly strong signal fading. It is also possible that the ρ/v_{eff} parameter is not appropriate for this interval, however when applying the algorithm with smaller ρ/v_{eff} we observed substantial deterioration in the results. Lastly, it is possible that the single-phase-screen model is inadequate over that portion of the data set.

4 | CONCLUSION

In this paper, we evaluated the impact of applying radio backpropagation to mitigate the occurrence of cycle slips under strong scintillation conditions. In our

simulations, we found that backpropagation essentially eliminated all cycle slips for signals with C/N_0 above 30 dB-Hz and for non-ionospheric Doppler residuals less than 0.02–0.03 m/s. Based on these results we conclude that, as long as the single-phase-screen model assumptions are accurate, backpropagation should be a very promising method for eliminating adverse effects that result from diffraction. We then applied the backpropagation to real scintillation data observed on the L1, L2, and L5 GPS signals. Our results reveal that backpropagation performs well (albeit not as flawlessly as predicted by the simulations). It is likely that the single-phase-screen assumption is not sufficiently realistic for this real-world case. It is also possible that there were non-ionospheric fluctuations remaining in the detrended phase. Future work might address the question of whether a technique employing multiple phase screens can improve the mitigation results presented in this paper and whether this approach might be adapted into a near-real-time algorithm.

REFERENCES

- Banville, S., Langley, R., Saito, S., & Yoshihara, T. (2010). Handling cycle slips in GPS data during ionospheric plasma bubble events. *Radio Science*, 45(06), 1–14. <https://doi.org/10.1029/2010RS004415>
- Breitsch, B. (2021). *Characterization and mitigation of GNSS carrier phase cycle slips* [Doctoral Dissertation]. University of Colorado at Boulder. <https://gnssrange.com/images/thesesAndDissertations/2021breitschBrian.pdf>
- Breitsch, B., Morton, Y. T., Rino, C., & Xu, D. (2020). GNSS carrier phase cycle slips due to diffractive ionosphere scintillation: Simulation and characterization. *IEEE Transactions on Aerospace and Electronic Systems*. <https://doi.org/10.1109/TAES.2020.2979025>
- Carrano, C. S., Groves, K. M., Caton, R. G., Rino, C. L., & Straus, P. R. (2011). Multiple phase screen modeling of ionospheric scintillation along radio occultation raypaths. *Radio Science*, 46(06), 1–14. <https://doi.org/10.1029/2010RS004591>
- de Oliveira Moraes, A., da Silveira Rodrigues, F., Perrella, W. J., & de Paula, E. R. (2012). Analysis of the characteristics of low-latitude GPS amplitude scintillation measured during solar maximum conditions and implications for receiver performance. *Surveys in Geophysics*, 33(5), 1107–1131. <https://doi.org/10.1007/s10712-011-9161-z>
- Ghafoori, F., & Skone, S. (2015). Impact of equatorial ionospheric irregularities on GNSS receivers using real and synthetic scintillation signals. *Radio Science*, 50(4), 294–317. <https://doi.org/10.1002/2014RS005513>
- Humphreys, T. E., Psiaki, M. L., Ledvina, B. M., Cerruti, A. P., & Kintner, P. M. (2010). Data-driven testbed for evaluating GPS carrier tracking loops in ionospheric scintillation. *IEEE Transactions on Aerospace and Electronic Systems*, 46(4), 1609–1623. <https://doi.org/10.1109/TAES.2010.5595582>
- Myer, G. T., & Morton, Y. T. (2018). Ionosphere scintillation effects on GPS measurements, a new carrier-smoothing technique, and positioning algorithms to improve accuracy. *Proc. of the 2018 International Technical Meeting of the Institute of Navigation (ITM 2018)*, Reston, VA. 420–439. <https://doi.org/10.33012/2018.15581>
- Rino, C. (2011). *The theory of scintillation with applications in remote sensing*. John Wiley & Sons.
- Rino, C., Breitsch, B., Morton, Y., Jiao, Y., Xu, D., & Carrano, C. (2018). A compact multi-frequency GNSS scintillation model. *NAVIGATION*, 65(4), 563–569. <https://doi.org/10.1002/navi.263>
- Rovira-Garcia, A., Juan, J. M., Sanz, J., & Gonzalez-Casado, G. (2020). The geodetic detrending technique: enabling high-accuracy navigation under scintillation. *Proc. of the IEEE International Conference on Wireless for Space and Extreme Environments (WiSEE 2020)*, Vicenza, Italy. 1–4. <https://doi.org/10.1109/WiSEE44079.2020.9262461>
- Sokolovskiy, S., Schreiner, W., Rocken, C., & Hunt, D. (2002). Detection of high-altitude ionospheric irregularities with GPS/MET. *Geophysical research letters*, 29(3), 3–1. <https://doi.org/10.1029/2001GL013398>
- Vadakke Veettil, S., Aquino, M., Marques, H. A., & Moraes, A. (2020). Mitigation of ionospheric scintillation effects on GNSS precise point positioning (PPP) at low latitudes. *Journal of Geodesy*, 94(2), 1–10. <https://doi.org/10.1007/s00190-020-01345-z>
- Wang, Y., Breitsch, B., & Morton, Y. T. J. (2020). A state-based method to simultaneously reduce cycle slips and noise in coherent GNSS-R phase measurements from open-loop tracking. *IEEE Transactions on Geoscience and Remote Sensing*. <https://doi.org/10.1109/TGRS.2020.3036031>

- Xu, D. (2019). *GPS equatorial ionospheric scintillation signals simulation, characterization, and estimation* [Doctoral Dissertation]. Colorado State University. <https://www.proquest.com/openview/874c9b6983adcb283cad1fc7aac064a0/1?pq-origsite=gscholar&cbl=18750&diss=y>
- Xu, D., Morton, Y. J., Rino, C. L., Carrano, C. S., & Jiao, Y. (2020). A two-parameter multifrequency GPS signal simulator for strong equatorial ionospheric scintillation: modeling and parameter characterization. *NAVIGATION*, 67(1), 1–15. <https://doi.org/10.1002/navi.350>

How to cite this article: Breitsch, B. & Morton, J. (2023). Mitigation of GNSS cycle slips due to scintillation using radio backpropagation. *NAVIGATION*, 70(3). <https://doi.org/10.33012/navi.593>